

## Article

# Supercritical Fluid-Assisted Fabrication of PDA-Coated Poly (L-lactic Acid)/Curcumin Microparticles for Chemo-Photothermal Therapy of Osteosarcoma

Zheng Zhao <sup>1,2</sup>, Shilu Chen <sup>1</sup>, Yao Xiao <sup>1</sup>, Maobin Xie <sup>3,4</sup> and Wen Yu <sup>5,\*</sup>

<sup>1</sup> State Key Laboratory of Advanced Technology for Materials Synthesis and Processing, Wuhan University of Technology, Wuhan 430070, China; zhengzhao@whut.edu.cn (Z.Z.); chinshiron@whut.edu.cn (S.C.); xyao@whut.edu.cn (Y.X.)

<sup>2</sup> Sanya Science and Education Innovation Park of Wuhan University of Technology, Sanya 572000, China

<sup>3</sup> Division of Engineering in Medicine, Department of Medicine, Brigham and Women's Hospital, Harvard Medical School, Cambridge, MA 02139, USA; mxie3@bwh.harvard.edu

<sup>4</sup> Department of Biomedical Engineering, School of Basic Medical Sciences, Guangzhou Medical University, The Sixth Affiliated Hospital of Guangzhou Medical University, Qingyuan People's Hospital, Guangzhou 511436, China

<sup>5</sup> Affiliated Hospital of Wuhan University of Technology, Wuhan 430070, China

\* Correspondence: yuwen@whut.edu.cn

**Abstract:** After traditional osteosarcoma resection, recurrence of tumor is still a major clinical challenge. The combination of chemotherapy and photothermal therapy (PTT) has great potential in improving therapeutic effect. However, the studies using polydopamine (PDA) as photothermal transducing agent to improve the anti-cancer activity of curcumin (CM)-loaded poly (L-lactic acid) (PLLA) microparticles (PLLA/CM) have seldom been investigated. In this study, we reported the synthesis of PDA-coated PLLA/CM microparticles (PDA-PLLA/CM) prepared by PDA coating on the surface of the PLLA/CM microparticles fabricated by solution-enhanced dispersion by supercritical CO<sub>2</sub> (SEDS) for chemo-photothermal therapy of osteosarcoma. The average particle sizes of PLLA/CM and PDA-PLLA/CM microparticles with a spherical shape were (802.6 ± 8.0) nm and (942.5 ± 39.5) nm, respectively. PDA-PLLA/CM microparticles exhibited pH- and near-infrared (NIR)-responsive release behavior to promote CM release in the drug delivery system. Moreover, PDA-PLLA/CM microparticles displayed good photothermal conversion ability and photothermal stability attributed to PDA coating. Additionally, the results of in vitro anti-cancer experiment showed that 500 µg/mL PDA-PLLA/CM microparticles had good anti-cancer effect on MG-63 cells and no obvious toxicity to MC3T3-E1 cells. After incubation with PDA-PLLA/CM microparticles for 2 days, NIR irradiation treatment improved the anti-cancer activity of PDA-PLLA/CM microparticles obviously and reduced the cell viability of osteosarcoma from 47.4% to 20.6%. These results indicated that PDA-PLLA/CM microparticles possessed a synergetic chemo-photothermal therapy for osteosarcoma. Therefore, this study demonstrated that PDA-PLLA/CM microparticles may be an excellent drug delivery platform for chemo-photothermal therapy of tumors.

**Keywords:** osteosarcoma therapy; microparticles; curcumin; synergetic chemo-photothermal therapy



**Citation:** Zhao, Z.; Chen, S.; Xiao, Y.; Xie, M.; Yu, W. Supercritical Fluid-Assisted Fabrication of PDA-Coated Poly (L-lactic Acid)/Curcumin Microparticles for Chemo-Photothermal Therapy of Osteosarcoma. *Coatings* **2022**, *12*, 524. <https://doi.org/10.3390/coatings12040524>

Academic Editor: Maria Cristina Tanzi

Received: 14 March 2022

Accepted: 11 April 2022

Published: 13 April 2022

**Publisher's Note:** MDPI stays neutral with regard to jurisdictional claims in published maps and institutional affiliations.



**Copyright:** © 2022 by the authors. Licensee MDPI, Basel, Switzerland. This article is an open access article distributed under the terms and conditions of the Creative Commons Attribution (CC BY) license (<https://creativecommons.org/licenses/by/4.0/>).

## 1. Introduction

Osteosarcoma is the most common primary malignant tumor of bone in children and adolescents, with a higher incidence in males than females [1,2]. Currently, the most common treatments for osteosarcoma include radiotherapy to kill the cancer cells to control its further metastasis, resection of the tumor tissue, and postoperative radiotherapy/chemotherapy [3]. However, due to the toxicity and low targeting of chemotherapy drugs, serious side effects can be caused to patients, such as cardiomyopathy, renal toxicity,

and bone marrow suppression [4,5]. Therefore, it is a key problem to achieve effective treatment of tumors and reduce the damage to normal cells.

Curcumin (CM), a natural polyphenol extracted from turmeric, has been widely reported for its anti-tumor, anti-bacterial, anti-diabetic, and anti-inflammatory properties [6,7]. CM could interact with enzymes, growth factor receptors, albumin, and other substances, such as glutathione S-transferase, hERG and cytochrome P450s [8–11]. However, several studies have shown that the toxicity can be avoided by controlling the amount of CM [12,13]. Furthermore, it has been proved that CM is safe at a high dose (8 g/day) in human clinical trials [14]. Although “Fake Cancer ‘Cures’ Consumers Should Avoid” released by FDA included CM, it only showed that some products containing CM did not exhibit effective anti-cancer ability and did not mean that CM has no anti-cancer effects. A large number of studies have confirmed that CM can inhibit the tumorigenic activity of various carcinogens in colon cancer, liver cancer, breast cancer, oral cancer, and other cancers [15–18]. Recent study has also shown that CM has good anti-cancer effect on osteosarcoma [12]. However, the bioavailability and therapeutic efficacy of CM are significantly reduced due to its poor water solubility and sensitivity to physiological pH conditions [16]. In recent years, many studies have reported the exploration of various materials to deliver CM to improve its water solubility, bioavailability, and absorption rate in vivo, such as nanoparticles, nanosheets and nanocomposites [19–21].

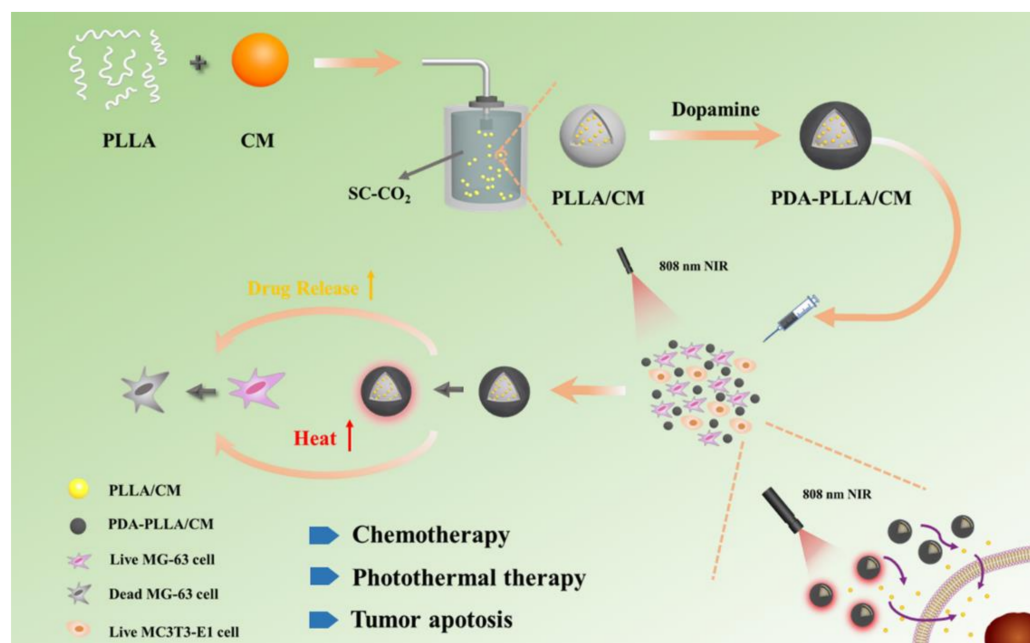
Currently, microparticles as a drug delivery system can improve the bioavailability and stability of drugs, which is an effective method to address the limitation of CM in tumor treatment [22]. At present, many different materials can be used as drug carriers, including liposomes, natural/artificial polymers, inorganic porous materials, etc. [23–25]. Due to the stable performance, biodegradability and biocompatibility of polymer materials, a variety of polymers, such as chitosan, alginate, poly (L-lactic acid) (PLLA), polyethylene glycol etc., have been applied to function as drug carriers [26–29]. Therein, PLLA microspheres, one of the most frequently used biodegradable synthetic polymer microspheres, have been designed to prepare drug loaded microspheres of small molecules, peptides and proteins [30–32]. According to differences between drugs, PLLA microspheres can be prepared by phase separation, melting, spray drying and other techniques [33–35]. The preparation process of phase separation method is complicated with many influencing factors. Therefore, it is difficult to control the quality of products. The melting method and spray drying technology require high temperature melting and are not suitable for drugs with poor thermal stability, as they inactivate the active substance.

Supercritical fluid granulation is a way to make use of the unique properties of supercritical fluid and realize the preparation of microparticles by controlling temperature and pressure, and supercritical carbon dioxide (scCO<sub>2</sub>) is the most widely used [36,37]. Supercritical CO<sub>2</sub> technology is one of the most promising methods to produce drug delivering microparticles. The process operates at a gentle temperature without destroying drug molecules and has no residual organic solvents in the final products [38,39]. The solution-enhanced dispersion by scCO<sub>2</sub> (SEDS) process has been widely used to prepare small size particles. The solution with dissolved solute is sprayed into supercritical CO<sub>2</sub> as anti-solvent, which can also enhance solution dispersion. The solvent diffuses into CO<sub>2</sub>, and the organic solvent is extracted into supercritical CO<sub>2</sub> very quickly, contributing to reducing the solubility of the solute. Then, the solute is precipitated out in the form of particles [40,41]. The smaller the diameter of the nozzle used is, the higher the injection speed is, and the larger the atomization degree is, the smaller the size of the droplets sprayed, so that the solvent in the solution can be more evenly removed by CO<sub>2</sub> reverse extraction [41].

Recently, photothermal therapy (PTT) has attracted wide attention due to its advantages of low side effects, repeatable treatment, short treatment time, and obvious effects [42]. PTT is a minimally invasive treatment that converts light energy into heat energy under the irradiation of an external light source such as near infrared (NIR) light, raising the temperature of the illuminated area to an effective therapeutic temperature to achieve

thermal ablation of tumors [43]. In the process of PTT, the temperature of the local tumor is the key to photothermal therapy. To achieve the ideal effect of photothermal therapy, the local temperature of tumor usually is required to reach about 45 °C to cause the heat injury of tumor cells and no damage to nearby normal tissue [44]. PTT cannot only cause death in cancer cells directly through raising the temperature, but also accelerate the release of drugs, playing a synergistic therapeutic effect. Therefore, the development of photothermal transducing agent with high Photothermal conversion rate, good water solubility and good biocompatibility has become the focus of research [42,45]. Polydopamine (PDA) is a biocompatible and biodegradable photothermal material, attracting extensive attention in the field of biomedical materials [46]. Compared with other photothermal transducing agents, PDA has higher photothermal conversion rate, good cell affinity and tissue adhesion, having a great prospect in the photothermal treatment of cancer [47]. A large amount of research has reported that PDA has been widely used as an efficient photothermal transducing agent and drug nanocarrier in PTT to improve anti-cancer efficacy [13,19–21]. PDA was used as a coating material to give some drug carriers the potential for photothermal therapy, protect the drug from premature release, and avoid rapid elimination from the body. PDA could be deposited on the surfaces of materials of various types and shapes by self-polymerization of dopamine under slightly alkaline conditions, such as nanosheets, nanoparticles and other materials [19,48]. Researchers have also reported that PDA was able to coat many drug-loaded microspheres, including CM-loaded microspheres [12,48]. However, studies using PDA-coated drug-loaded PLLA microparticles for the photothermal treatment of osteosarcoma have seldom been performed.

Herein, we report a compound drug-loaded microsphere, encapsulating CM in PLLA by the SEDS process to obtain PLLA/CM microparticles, which are then coated by PDA on the surface, for treating osteosarcoma with a chemo-photothermal therapy (Scheme 1). The morphology, size, CM loading efficiency, in vitro release behavior and photothermal properties of the PDA-PLLA/CM microparticles are studied in this article. The synergistic chemo-photothermal therapy effects of PDA-PLLA/CM microparticles were further studied by in vitro experiments. This study provides a new strategy for the use of the SEDS process and a synergistic chemo-photothermal therapy for promoting osteosarcoma cell apoptosis by drug-loaded microparticles.



**Scheme 1.** The scheme of the construction route of PDA-PLLA/CM and the chemo-photothermal synergistic therapy of osteosarcoma.

## 2. Materials and Methods

### 2.1. Materials

PLLA (100 kDa, 98%, Macklin, Shanghai, China), CM (Aladdin Shanghai, China), dopamine hydrochloride (Aladdin, Shanghai, China), Tris-HCl solution (pH 8.5 Beyotime Biotechnology, Jiangsu, China), CO<sub>2</sub> (99.9%, Wuhan Xiangyun, Wu Han, China), Dichloromethane (DCM, Aladdin, Shanghai, China), ethanol (Aladdin, Shanghai, China), MTS dye (Promega Biotech, Beijing, China) and Calcein-AM/PI Double Stain Kit (Beijing Solarbio Science & Technology, Beijing, China) were used as obtained. The MC3T3-E1 cells and MG-63 cells were supplied by China Center for Type Culture Collection.

### 2.2. Methods

#### 2.2.1. Synthesis of PLLA/CM Microparticles by SEDS Process

Firstly, PLLA (200 mg) and CM (50 mg) were dissolved in DCM (50 mL). After stirring (1000 r/min) for 2 h, drug-loaded microparticles were prepared by using SEDS technology. The CO<sub>2</sub> is delivered by a pump through a special tube into a pressure vessel. When the CO<sub>2</sub> was preheated to 35 °C and reached 10 MPa, keep CO<sub>2</sub> flow rate (20 g/min) and control the system pressure. The PLLA/CM solution is then injected at a flow rate (1 mL/min). After all the solution was transported, CO<sub>2</sub> was pumped to keep flow in the system under the same conditions for 30 min for removing the residual organic solvents. Finally, PLLA/CM microparticles were then collected on the bottom of the high-pressure vessel.

#### 2.2.2. Preparation of PDA-PLLA/CM Microparticles

PLLA/CM (0.5 mg/mL) was dispersed in deionized water and ultrasound treatment was performed in an ice bath for 15 min. After maximizing dispersion, dopamine hydrochloride (2.5 mg/mL) and Tris-HCl (1%) were successively added to the solution, and mixed at room temperature for 2 h. The solution gradually changed from light yellow to black. The PDA-PLLA/CM microparticles were centrifuged (10,000 rpm, 30 min) and washed 3 times and then finally lyophilized under vacuum.

#### 2.2.3. Characterization of PDA-PLLA/CM Microparticles

Fourier transform-infrared spectroscopy was performed using Nicolet 6700 from USA to study the component analysis of the prepared microparticle samples. X-ray diffraction (XRD, Bruker AXS, Billerica, MA, USA) was performed using D8 Advance from Germany to evaluate the phase structure of various samples. Field emission-scanning electron microscopy (FE-SEM, JEOL, Tokyo, Japan) was conducted using S-4800 from Japan to observe the surface morphology of the materials. The microscopic morphology, size and distribution of samples can be inspected with different magnification. The hydrodynamic diameter of the microparticles were measured with a Malvin laser particle size analyzer (Mastersizer 2000, Malvern, Shanghai, China). Ultraviolet (UV)-spectrophotometer (SHIMADZU, Kyoto, Japan) was used to record the absorbance of the PLLA, PLLA/CM, PDA-PLLA and PDA-PLLA/CM microparticles.

#### 2.2.4. Drug Loading and Controlled Release Study

The drug loading efficiency of the PDA-PLLA/CM microparticles was evaluated by the following protocol. The PDA-PLLA/CM microparticles were dissolved in DCM and were further dissolved in ethanol ( $v/v = 1/99$ ) and subsequently sonicated for 15 min. After centrifugation (10,000 r/min) for 15 min, the amount of CM in the supernatant was quantified according to the optical density at 425 nm. The CM loading efficiency was calculated by the following equation:

$$DL(CM)(\%) = \frac{\text{the amount of CM in the microparticles}}{\text{the weight of the microparticles}} \times 100\% \quad (1)$$

The amount of drug release was evaluated by the following method. PDA-PLLA/CM microparticles (1 mg/mL) were incubated into the mixed solution of phosphate-buffered saline (PBS) and Tween 80 (1%) with pH = 7.4 and 5.5, respectively. A 3 mL volume of sample solution was placed into the dialysis bag, replenished in different buffers (30 mL), then shaken at 100 rpm and kept at 37 °C. At the dedicated time intervals, 4 mL supernatant was collected with the replacement of 4 mL buffer with the same pH value. In addition, before and after 808 nm NIR irradiation (10 min), the CM release amount was detected at specific time points (10 h, 23 h, 48 h, 72 h), showing NIR-responsive release behavior. Combining the UV-Vis spectrophotometry and the standard curve of CM, the drug release amount was calculated and the cumulative release curve was drawn. Three parallel groups were set for all samples.

### 2.2.5. In Vitro Photothermal Performance

The temperature of PDA-PLLA/CM microparticles with different concentrations was recorded to study the temperature rise caused by 808 nm NIR laser (MDL-H-808-5W-BJ00440, Changchun New Industries Optoelectronics Tech. Co., Changchun, China). PDA-PLLA/CM microparticles were dispersed in deionized water (60, 125, 250, 500 and 1000 µg/mL) with 1.3 W/cm<sup>2</sup> for 10 min. In addition, the same volume of pure deionized water was used as control. The temperature changes of the microparticles (500 µg/mL) were also recorded with different laser power (1.0, 1.3, 1.5 W/cm<sup>2</sup>) for 10 min. Meanwhile, in order to study the photothermal stability, the PDA-PLLA/CM microparticles (500 µg/mL) were irradiated with a NIR laser for 5 cycles in 1200 s intervals. During the above experiment, the temperature of the solution was recorded using a liquid crystal thermometer every 1 min. The photothermal conversion efficiency ( $\eta$ ) was calculated using a reported method by the following equations [49]:

$$\eta = \frac{hS(T_{\max} - T_{\text{room}}) - hS(T_{\max, \text{water}} - T_{\text{room}})}{I(1 - 10^{-A_{808}})} \quad (2)$$

$$\tau_s = \frac{mC}{hS} \quad (3)$$

According to Equation (3), the value of  $hS$  could be calculated.  $h$  refers to the heat transfer coefficient and  $S$  refers to the area of the container.  $I$  represents the NIR laser power and  $A_{808}$  is the absorbance of PDA-PLLA/CM microparticles (500 µg/mL) at 808 nm. In addition,  $m$  is the mass of the sample solution,  $C$  is the heat capacity ( $C_{\text{water}} = 4.2 \text{ J}/(\text{g} \cdot ^\circ\text{C})$ ).

### 2.2.6. Cell Culture and Proliferation

MG-63 cells (human osteosarcoma cells) were cultured with MEM medium consisting of 10% fetal bovine serum (FBS) and 1% penicillin/streptomycin (P.S). MC3T3-E1 cells (mouse pre-osteoblast cells) were cultured in  $\alpha$ -MEM medium with 10% FBS and 1% P.S. The cells were then incubated in a humidified atmosphere containing 95% air and 5% CO<sub>2</sub> at 37 °C.

### 2.2.7. In Vitro Biocompatibility and Antitumor Effect

MTS assay was used for both antitumor effect of the PDA-PLLA/CM microparticles on MG-63 cells and no toxicity on MC3T3-E1 cells. The MG-63 and MC3T3-E1 cells were preincubated for 24 h. Then, the cells were co-cultivated with various samples for 48 h (or 1, 3, 5 days). Subsequently, the culture medium was discarded, the cells were washed three times with PBS, 50 µL of MTS solution and 250 µL of fresh medium were added into each well. After incubating for 4 h, the absorbance values were recorded at 490 nm using by a

microplate reader from Thermo Scientific. The cellular viability was determined by the following equation:

$$\text{Cell viability (\%)} = \frac{\text{absorbance of experiment cells}}{\text{absorbance of control}} \times 100\% \quad (4)$$

In addition, a Live/Dead assay was applied to further investigate the effects of the different samples and concentrations on MG-63 and MC3T3-E1 cells. After being co-cultivated with different microparticles for 48 h, the cells were stained using a Calcein-AM/PI double staining kit for 30 min. The morphology of the cells was examined using a fluorescent microscope from OLYMPUS (Tokyo, Japan).

#### 2.2.8. In Vitro Chemo-Photothermal Therapy Evaluation

The effect of the chemo-photothermal therapy was evaluated using the activity of MG-63 cells treated with PLLA, CM (75 µg/mL), PLLA/CM, PDA-PLLA, PDA-PLLA/CM microparticle solutions at 500 µg/mL under NIR laser irradiation. The cells were seeded on 48-well plates and then co-cultured with different samples for 48 h. Subsequently, the cells were irradiated using 808 nm NIR laser with an intensity of 1.3 W/cm<sup>2</sup> (10 min) and placed in an incubator for 12 h. The activity of MG-63 cells was determined by MTS reagent and Calcein-AM/PI Double Stain Kit (Beijing Solarbio Science & Technology, Beijing, China).

#### 2.2.9. Statistical Analysis

All the data are given as mean values ± standard deviation (SD) from at least three independent samples. Statistical analysis was conducted using SPSS software (version 19.0) to evaluate the significance. (\*) represents *p*-value < 0.05, (\*\*) represents *p*-value < 0.01, and (\*\*\*) represents *p*-value < 0.001.

### 3. Results and Discussion

#### 3.1. Synthesis and Characterization of PDA-PLLA/CM Microparticles

The FTIR and XRD patterns of PLLA, CM, PLLA/CM and PDA-PLLA/CM microparticles were used to verify that CM was loaded on PLLA and PDA layer was coated on PLLA/CM. As shown in Figure 1A, the pertinent peaks at 1756 cm<sup>-1</sup> in the FTIR spectra of PLLA, PLLA/CM and PDA-PLLA/CM microparticles corresponded to the C=O stretching vibration in PLLA. The absorption band in the range of 1600 and 1400 cm<sup>-1</sup> could be ascribed to aromatic C=C stretching vibration connecting with CM [36], indicating loading of CM in PLLA/CM and PDA-PLLA/CM microparticles. After modification by PDA, the absorption peak of the bending vibration of N-H at 1509 cm<sup>-1</sup> appeared in the FTIR spectra of PDA-PLLA/CM. The XRD patterns of PLLA, CM, PLLA/CM and PDA-PLLA/CM microparticles are shown in Figure 1B. The characteristic high-intensity peaks at 2θ = 12.4°, 14.6°, 16.7° and 19.0° were attributed to PLLA. The characteristic diffraction peaks attributed to CM at 8.8° and 17.2° were observed in PDA-PLLA/CM microparticles, indicating the presence of CM. From the FTIR and XRD analysis results, it can be further confirmed that the prepared microparticles are PDA-PLLA/CM composite microparticles.

The morphology of PLLA/CM and PDA-PLLA/CM microparticles was characterized by SEM. As shown in Figure 2A,C, microparticles before and after being coated with PDA both presented a spherical morphology. It was observed that the surface of PLLA/CM was smooth, while the surface of microparticles after modification by PDA was rough. Malvern laser particle size analyzer was used to obtain the microparticle size and size distribution. From Figure 2B,D, the average particle sizes of PLLA/CM and PDA-PLLA/CM microparticles were (802.6 ± 8.0) nm and (942.5 ± 39.5) nm, respectively. Compared with PLLA/CM microparticles, the average sizes of PDA-PLLA/CM microparticles was larger, which may be contributed to the PDA layers forming a covering over the CM-loaded PLLA microparticles.

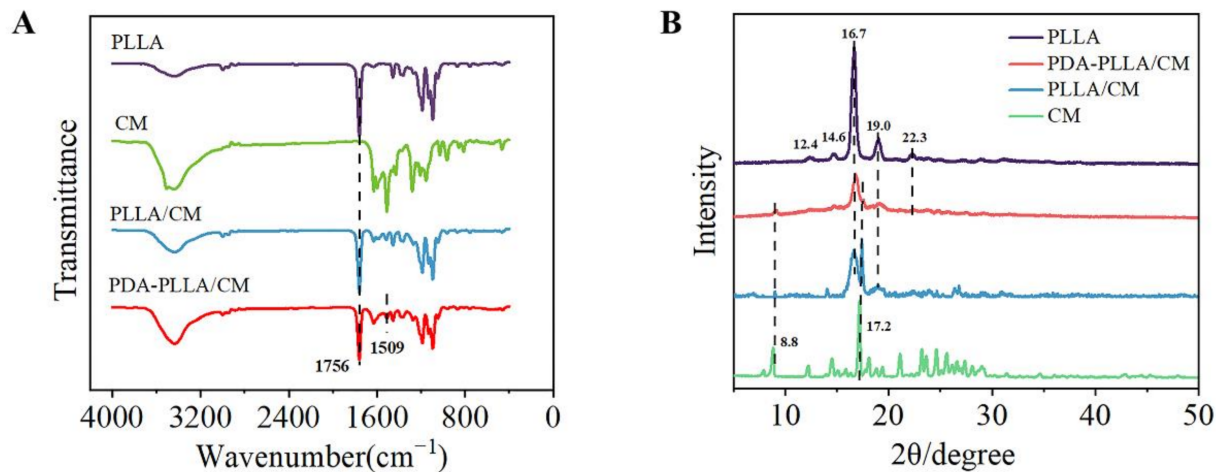


**Figure 1.** (A) FTIR spectra, (B) XRD patterns of PLLA, CM, PLLA/CM and PDA-PLL/CM microparticles.

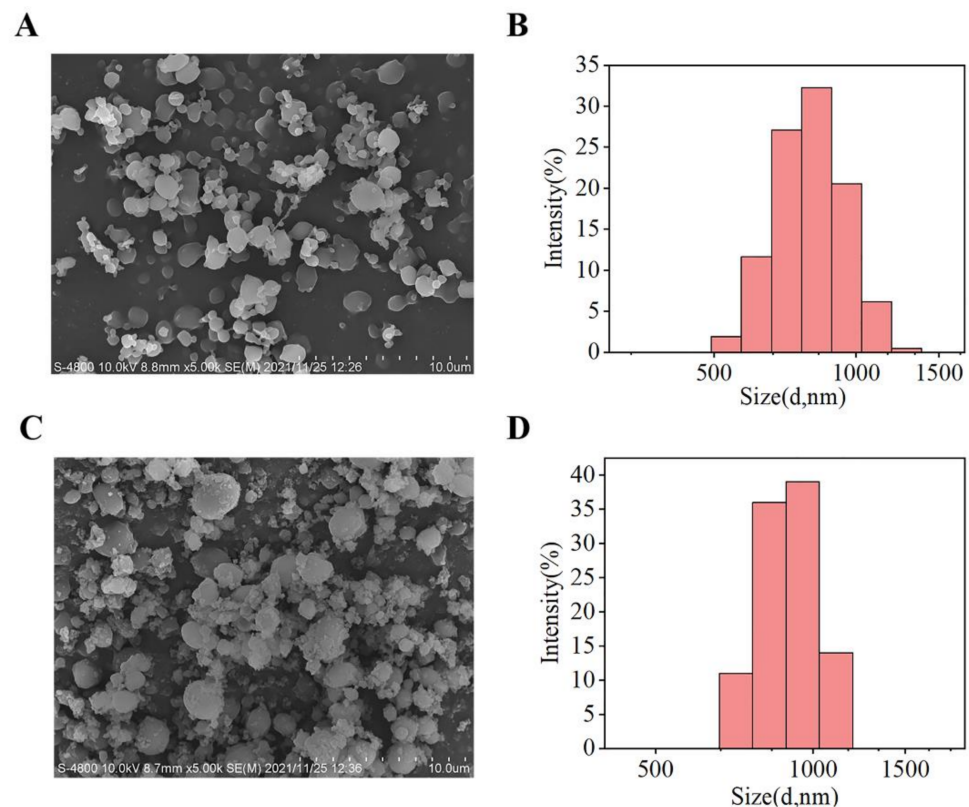


**Figure 2.** Morphology character of samples. (A) SEM images of PLLA/CM microparticles. (B) Size distribution of PLLA/CM microparticles. (C) SEM images of PDA-PLL/CM microparticles. (D) Size distribution of PDA-PLL/CM microparticles.

### 3.2. Drug Loading and Responsive Release

As shown in Figure 3A, the UV absorption spectral of the samples was used to calculate the drug loading efficiency (DLE) of PLLA/CM, PDA-PLL/CM microparticles. PLLA and PDA-PLL microparticles had no obvious characteristic peaks within the detection range of 300–600 nm. After the CM loading process, a characteristic absorption peak appeared at 425 nm in the spectral of PLLA/CM and PDA-PLL/CM microparticles, proving that CM was successfully loaded on the microparticles. The CM loading rates was 15.6% calculated by the standard curve of CM and corresponding formula for the quantitative analysis.

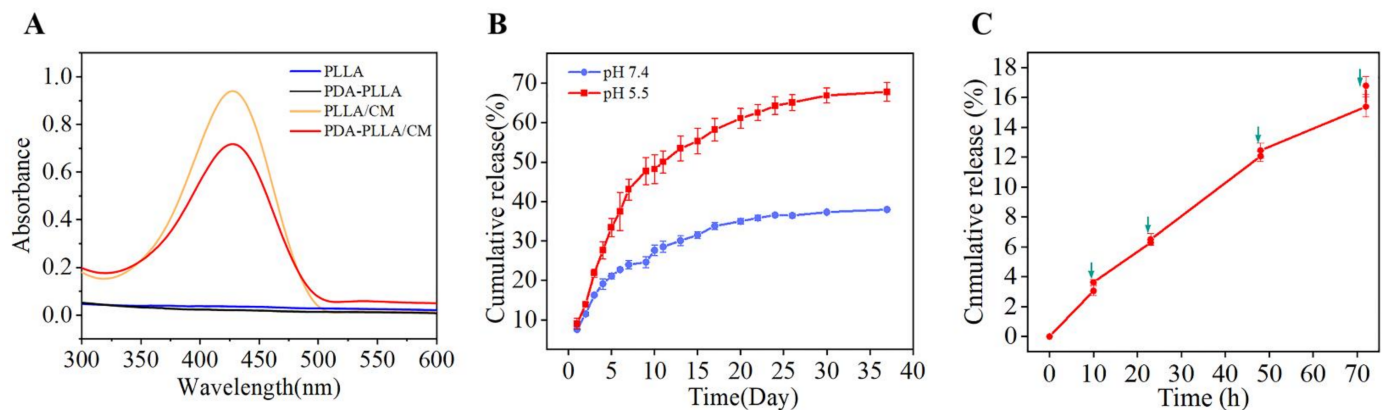


**Figure 3.** Drug-loading character of microparticles. (A) UV–Vis absorption spectra of PLLA/CM and PDA-PLL/CM microparticles for CM (425 nm). (B) CM release curves under different pH. (C) NIR-response release of CM for 10 min (pH 5.5, 1.3 W/cm<sup>2</sup>).

As depicted in Figure 3B, the CM release behavior of PDA-PLL/CM microparticles in different condition was investigated in vitro. PDA-PLL/CM microparticles exhibited a typical pH-responsive release behavior. The release rate of CM accelerated from 24.9% to 58.7% when the pH value changed from 7.4 to 5.5 after 30 days. The similar studies have reported that PDA could more easily degrade from the surface of microparticles after immersed in the acid media, promoting drug release [48,50]. Moreover, after NIR irradiation for 10 min, burst release of CM could be found (Figure 3C). This may be caused by the increase in local temperature generated by PDA after irradiation, accelerating the molecular motion. The pH- and NIR-responsive drug release could make PDA-PLL/CM microparticles a potential option for synergic tumor chemo-photothermal therapy.

### 3.3. Photothermal Property Evaluation

To demonstrate the photothermal properties of PDA-PLL/CM microparticles, the temperature changes were recorded under NIR laser irradiation at room temperature. PDA-PLL/CM microparticles exhibited excellent photothermal conversion properties, attributing to the coating of PDA. With increasing microparticle concentration and radiation time, the temperature of the solution increased at a power density of 1.3 W/cm<sup>2</sup> (Figure 3A). The temperature of the microparticles at concentrations of 250 µg/mL, 500 µg/mL, and 1000 µg/mL reached 46.5 °C, 51.7 °C and 60.8 °C after 10 min, respectively. Moreover, it was revealed that the temperature of the microparticles also changed with different power densities in Figure 4B. The ultimate temperature of PDA-PLL/CM microparticles (500 µg/mL) was increased rapidly, with a power intensity increase from 1 to 1.5 W/cm<sup>2</sup>. It has been proved that temperatures of over 44 °C can induce apoptosis by cell damage [51]. Furthermore, the temperature of 5 laser on/off cycles was examined at 1.3 W/cm<sup>2</sup> (Figure 4C). It was found that the maximum temperature of all cycles reached at 51.2 ± 0.7 °C, and there was no obvious reduction. Therefore, the photothermal effect would not weaken with increased radiation time, indicating that the microparticles had splendid photostability provided by PDA [48]. In addition, the photothermal conversion efficiency ( $\eta$ ) could be calculated to be 18.4% from a cooling curve (Figure 4C) and the thermal time constant ( $\tau_s = 242.89$ ) (Figure 4D). This value is basically consistent with that presented in previous studies, confirming that the photothermal conversion process of PDA has high efficiency [13].

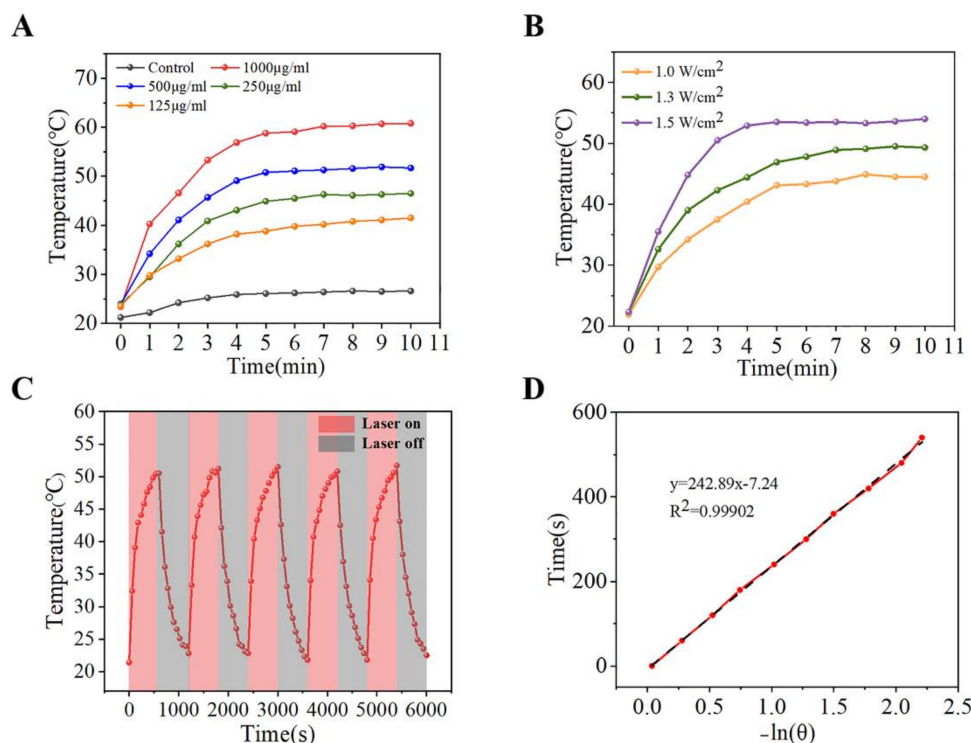


**Figure 4.** Photothermal properties of PDA-PLLA/CM microparticles. (A) Temperature variation at different concentrations under 808 nm irradiation ( $1.3 \text{ W/cm}^2$ ) for 10 min, (B) at different powers of irradiation ( $500 \text{ µg/mL}$ ) for 10 min, and (C) over 5 irradiation cycles (808 nm,  $500 \text{ µg/mL}$ ,  $1.3 \text{ W/cm}^2$ ). (D) Fitting curves of the time logarithm of the temperature during the cooling process.

### 3.4. In Vitro Anti-Cancer of PDA-PLLA/CM Microparticles

The in vitro anti-cancer effects of PDA-PLLA/CM microparticles with different concentrations are shown in Figure 5A. Obviously, PDA-PLLA/CM microparticles with concentrations ranging from  $30$  to  $60 \text{ µg/mL}$  had no significant toxicity to MG-63 cells. When the concentration of the microparticles increased from  $125 \text{ µg/mL}$  to  $500 \text{ µg/mL}$ , the cell survival rate decreased from  $71.8\%$  to  $45.4\%$ . These results suggest that the anti-cancer effect of PDA-PLLA/CM microparticles is concentration dependent. In addition to ensuring drug efficacy, in vitro cytotoxicity should also be considered before beginning human application. Therefore, the effect of PDA-PLLA/CM microparticles with different concentrations on the viability of MC3T3-E1 cells was investigated (Figure 5B). At concentrations lower than  $500 \text{ µg/mL}$ , the activity of PDA-PLLA/CM microparticles on MC3T3-E1 cells was not significantly decreased. However, the cell survival rate of MC3T3-E1 cells decreased to  $86.5\%$  at the concentration of increasing to  $1000 \text{ µg/mL}$ .

Based on the above results,  $500 \text{ µg/mL}$  PDA-PLLA/CM microparticles had outstanding anti-cancer activity, and no obvious cytotoxicity to MC3T3-E1 cells was identified. As demonstrated in previous studies, the anti-cancer activity of CM could be attributed to the inhibition of hypoxia-induced proliferation and invasion of MG-63 osteosarcoma cells by downregulating the expression of Notch1 and activating miR-125a/ERR $\alpha$  Signal Pathway by downregulating ERR $\alpha$  gene expression and upregulating miR-125a level [52,53]. It has also been shown in other studies that tumor cells are more sensitive to the cytotoxicity of CM than normal cells [12,13,48]. Therefore, PDA-PLLA/CM microparticles with a concentration of  $500 \text{ µg/mL}$  were selected to study the effects of different culture time on the viability of MG-63 and MC3T3-E1 cells. As shown in Figure 5C, the PLLA and PDA-PLLA microparticles exhibited no influence on the activity of MG-63 cells after co-cultured for 1, 3 and 5 days, while CM, PLLA/CM and PDA-PLLA/CM microparticles could markedly decrease the activity of MG-63 cells. The anti-cancer effects of PDA-PLLA/CM microparticles increased with the prolongation of co-culture time, suggesting that the microparticles has a

long-term and stable anti-cancer effect. This may be a result of the effect of the stable CM release from PDA-PLLA/CM microparticles on cells. From Figure 5D, the PDA-PLLA/CM microparticles had a good cytocompatibility with MC3T3-E1 cells. With the extension of culture time, the proliferation of MC3T3-E1 cells was not significantly inhibited by PDA-PLLA/CM microparticles. Consequently, PDA-PLLA/CM microparticles have good application prospects in the treatment of bone tumor.

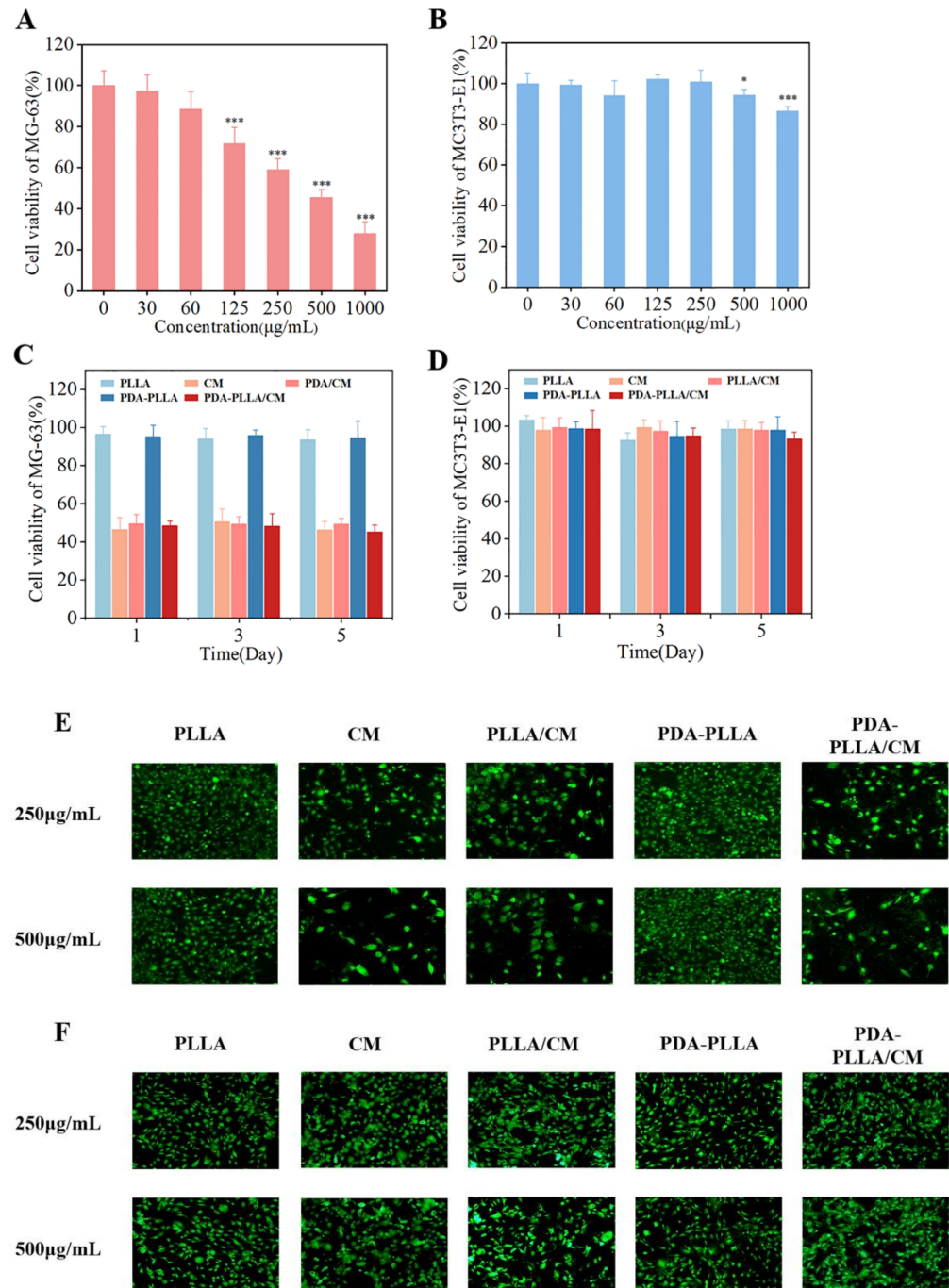


**Figure 5.** (A,B) Cell viability after being co-cultured with PDA-PLLA/CM microparticles at different concentrations for 48 h. (C,D) After being treated with different samples for 1, 3, 5 days. (E,F) Fluorescence staining images of MG-63 and MC3T3-E1 cells incubation with different samples. (PLLA, PLLA/CM, PDA-PLLA and PDA-PLLA/CM microparticles, 500 µg/mL; CM, 75 µg/mL). (\*  $p$ -value < 0.05, \*\*\*  $p$ -value < 0.001).

The fluorescence images of the staining assay (Figure 5E) show that in comparison with culturing with 500  $\mu\text{g}/\text{mL}$  PDA-PLLA/CM microparticles, MG-63 cells were more obviously ablated when co-cultured with 500  $\mu\text{g}/\text{mL}$  sample solution for 48 h, which is consistent with the above results. Furthermore, as shown in Figure 5F, even at a concentration of 500  $\mu\text{g}/\text{mL}$ , PLLA, CM (75  $\mu\text{g}/\text{mL}$ ), PLLA/CM, PDA-PLLA and PDA-PLLA/CM microparticles had good cytocompatibility, further demonstrating that all samples had no obvious toxicity for osteoblasts.

### 3.5. In Vitro Chemo-Photothermal Therapy Effect

To study the effects of PDA-PLLA/CM microparticles on tumor cells under NIR irradiation, MG-63 cells were incubated with PLLA, CM, PLLA/CM, PDA-PLLA and PDA-PLLA/CM microparticles with or without NIR laser radiation. As shown in Figure 6A, PLLA had almost no effect on the viability of MG-63 cells before and after NIR treatment, verifying the safety of the laser. When MG-63 cells were co-cultured with CM and PLLA/CM before and after NIR irradiation, the cell activity was about 48.1% and 44.7%, 48.2% and 47.4%, respectively. As shown in Figure 3C, the heat could accelerate CM release to induce the tumor cells apoptosis with NIR irradiation. The viability of MG-63 cell was 91.1% and 49.7% when incubated with the PDA-PLLA and PDA-PLLA/CM microparticles without NIR irradiation, further confirming the effective loading of CM. Moreover, after being co-cultured with PDA-PLLA/CM microparticles with NIR irradiation, cell activity could be reduced to only 20.6%, indicating that the therapeutic effect was greatly improved. It has been reported that a “suppressive hyperthermia” (45–48  $^{\circ}\text{C}$ ) could cause rapid necrotic death in cancer cells that are resistant to standard hyperthermia [54].

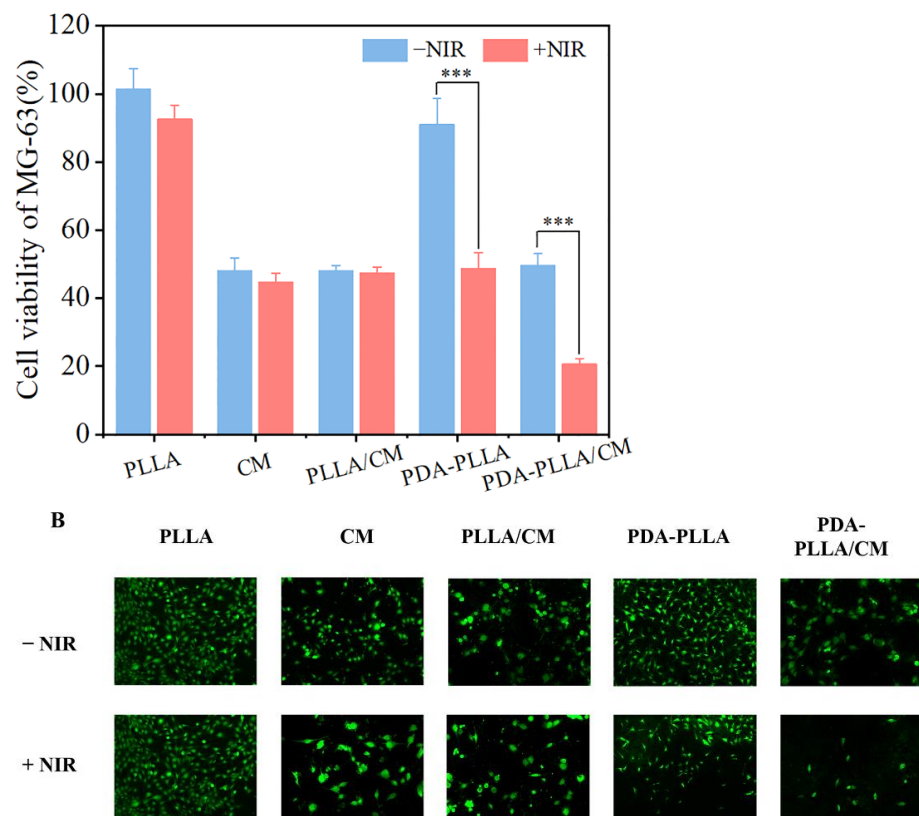


**Figure 6.** (A) Cell viability of MG-63 cells after being cultured with PLLA, PLLA/CM, PDA-PLLA and PDA-PLLA/CM microparticles at the same CM concentration level with or without NIR irradiation (PLLA, PLLA/CM, PDA-PLLA and PDA-PLLA/CM microparticles, 500  $\mu\text{g}/\text{mL}$ ; CM, 75  $\mu\text{g}/\text{mL}$ ). (B) Fluorescence staining images of MG-63 cells with or without NIR irradiation (1.3  $\text{W}/\text{cm}^2$ ) for 10 min. (\*\*\*)  $p$ -value < 0.001).

Live cells stained with fluorescent dye were observed to further investigate the growth of cells. As shown in Figure 6B, under the NIR irradiation, the number of live cells in PDA-PLLA/CM microparticles group was obviously less than in the CM and PLLA/CM microparticle groups. Therefore, it could also be confirmed that NIR irradiation could enhance antitumor effects significantly of the PDA-PLLA/CM microparticles.

#### 4. Conclusions

In conclusion, we report a composite drug-loaded microsphere, which was synthesized by the SEDS process and then functionalized by PDA, for the chemo-photothermal treatment of osteosarcoma. The PLLA/CM microparticles with a size of  $(802.6 \pm 8.0)$  nm prepared by SEDS technology improved the bioavailability of CM. The PDA-PLLA/CM microparticles with a size of  $(942.5 \pm 39.5)$  nm were able to realize pH- and near-infrared (NIR) responsive release of CM. PDA had a strong thermal response to 808 nm NIR radiation, not only providing photothermal treatment for tumor particles, but also promoting the release of CM. In vitro anti-cancer experiment results showed that the growth of MG-63 cells was effectively inhibited by PDA-PLLA/CM microparticles and the activity of MC3T3-E1 cells was not affected. In addition, the cell viability of MG-63 was reduced from 47.4% to only 20.6% for chemo-photothermal therapy incubated with 500  $\mu\text{g}/\text{mL}$  PDA-PLLA/CM microparticles before and after NIR irradiation. Therefore, PDA-PLLA/CM microparticles reported in this study provides a new strategy for the application of SEDS technology, and also has great potential for synergetic chemo-photothermal therapy for osteosarcoma.

**Author Contributions:** Z.Z.: conceptualization, formal analysis, writing—review & editing, supervision, project administration, funding acquisition; S.C.: writing—original draft, methodology, writing—review & editing, formal analysis, software; Y.X.: writing—review & editing, methodology, supervision; M.X.: investigation, supervision, validation; W.Y.: data curation, supervision, writing—review & editing. All authors have read and agreed to the published version of the manuscript.

**Funding:** This study was funded by the National Natural Science Foundation of China (52073220), Sanya Science and Education Innovation Park of Wuhan University of Technology (2021KF0017), State Key Laboratory of Advanced Technology for Materials Synthesis and Processing (Wuhan University of Technology) (2021-KF-2), and Young Top Notch Talents Fund of Wuhan University of Technology (471–40120093).

**Institutional Review Board Statement:** Not applicable.

**Informed Consent Statement:** Not applicable.

**Data Availability Statement:** Not applicable.

**Conflicts of Interest:** The authors declare no conflict of interest.

#### References

1. Bozorgi, A.; Sabouri, L. Osteosarcoma, personalized medicine, and tissue engineering; an overview of overlapping fields of research. *Cancer Treat. Res. Commun.* **2020**, *27*, 100324. [[CrossRef](#)] [[PubMed](#)]
2. Harrison, D.J.; Geller, D.S.; Gill, J.D.; Lewis, V.O.; Gorlick, R. Current and future therapeutic approaches for osteosarcoma. *Expert Rev. Anticancer Ther.* **2018**, *18*, 39–50. [[CrossRef](#)] [[PubMed](#)]
3. Isakoff, M.S.; Bielack, S.S.; Meltzer, P.; Gorlick, R. Osteosarcoma: Current Treatment and a Collaborative Pathway to Success. *J. Clin. Oncol.* **2015**, *33*, 3029. [[CrossRef](#)]
4. Djunic, I.; Elezovic, I.; Marinkovic, M.; Suvajdzic-Vukovic, N.; Tomin, D.; Jankovic, G.; Bila, J.; Antic, D.; Vidovic, A.; Neskovic, B.; et al. Osteolytic lesions marker in multiple myeloma. *Med. Oncol.* **2011**, *28*, 237–240. [[CrossRef](#)]
5. Tennant, D.A.; Duran, R.V.; Gottlieb, E. Targeting metabolic transformation for cancer therapy. *Nat. Rev. Cancer* **2010**, *10*, 267–277. [[CrossRef](#)] [[PubMed](#)]
6. Mahmood, K.; Zia, K.M.; Zuber, M.; Salman, M.; Anjum, M.N. Recent developments in curcumin and curcumin based polymeric materials for biomedical applications: A review. *Int. J. Biol. Macromol.* **2015**, *81*, 877–890. [[CrossRef](#)]
7. Meng, Z.; Liu, Y.; Xu, K.; Sun, X.; Yu, Q.; Wu, Z.; Zhao, Z. Biomimetic Polydopamine-Modified Silk Fibroin/Curcumin Nanofibrous Scaffolds for Chemo-photothermal Therapy of Bone Tumor. *ACS Omega* **2021**, *6*, 22213–22223. [[CrossRef](#)]
8. Hu, C.-W.; Sheng, Y.; Zhang, Q.; Liu, H.-B.; Xie, X.; Ma, W.-C.; Huo, R.; Dong, D.-L. Curcumin inhibits hERG potassium channels in vitro. *Toxicol. Lett.* **2012**, *208*, 192–196. [[CrossRef](#)]

9. Komal, K.; Chaudhary, S.; Yadav, P.; Parmanik, R.; Singh, M. The Therapeutic and Preventive Efficacy of Curcumin and Its Derivatives in Esophageal Cancer. *Asian Pac. J. Cancer Prev.* **2019**, *20*, 1329–1337. [[CrossRef](#)]
10. Piper, J.T.; Singhal, S.S.; Salameh, M.S.; Torman, R.T.; Awasthi, Y.C.; Awasthi, S. Mechanisms of anticarcinogenic properties of curcumin: The effect of curcumin on glutathione linked detoxification enzymes in rat liver. *Int. J. Biochem. Cell Biol.* **1998**, *30*, 445–456. [[CrossRef](#)]
11. Oetari, S.; Sudiby, M.; Commandeur, J.N.; Samhoedi, R.; Vermeulen, N.P. Effects of curcumin on cytochrome P450 and glutathione S-transferase activities in rat liver. *Biochem. Pharmacol.* **1996**, *51*, 39–45. [[CrossRef](#)]
12. Sun, X.; Meng, Z.; Yu, Q.; Wang, X.; Zhao, Z. Engineering PDA-coated CM-CS nanoparticles for photothermo-chemotherapy of osteosarcoma and bone regeneration. *Biochem. Eng. J.* **2021**, *175*, 108138. [[CrossRef](#)]
13. Wang, Y.-C.; Dai, H.-L.; Li, Z.-H.; Meng, Z.-Y.; Xiao, Y.; Zhao, Z. Mesoporous polydopamine-coated hydroxyapatite nanocomposites for ROS-triggered nitric oxide-enhanced photothermal therapy of osteosarcoma. *J. Mater. Chem. B* **2021**, *9*, 7401–7408. [[CrossRef](#)] [[PubMed](#)]
14. Lao, C.D.; Ruffin, M.T.; Normolle, D.; Heath, D.D.; Murray, S.I.; Bailey, J.M.; Boggs, M.E.; Crowell, J.; Rock, C.L.; Brenner, D.E. Dose escalation of a curcuminoid formulation. *BMC Complementary Altern. Med.* **2006**, *6*, 10. [[CrossRef](#)] [[PubMed](#)]
15. Cao, J.; Liu, Y.; Jia, L.; Zhou, H.-M.; Kong, Y.; Yang, G.; Jiang, L.-P.; Li, Q.-J.; Zhong, L.-F. Curcumin induces apoptosis through mitochondrial hyperpolarization and mtDNA damage in human hepatoma G2 cells. *Free. Radic. Biol. Med.* **2007**, *43*, 968–975. [[CrossRef](#)] [[PubMed](#)]
16. Dhillon, N.; Aggarwal, B.B.; Newman, R.A.; Wolff, R.A.; Kunnumakkara, A.B.; Abbruzzese, J.L.; Ng, C.S.; Badmaev, V.; Kurzrock, R. Phase II trial of curcumin in patients with advanced pancreatic cancer. *Clin. Cancer Res.* **2008**, *14*, 4491–4499. [[CrossRef](#)] [[PubMed](#)]
17. Johnson, J.J.; Mukhtar, H. Curcumin for chemoprevention of colon cancer. *Cancer Lett.* **2007**, *255*, 170–181. [[CrossRef](#)]
18. Lelli, D.; Sahebkar, A.; Johnston, T.P.; Pedone, C. Curcumin use in pulmonary diseases: State of the art and future perspectives. *Pharmacol. Res.* **2017**, *115*, 133–148. [[CrossRef](#)]
19. Liu, F.; Lin, L.; Zhang, Y.; Sheng, S.; Wang, Y.; Xu, C.; Tian, H.; Chen, X. Two-dimensional nanosheets with high curcumin loading content for multimodal imaging-guided combined chemo-photothermal therapy. *Biomaterials* **2019**, *223*, 119470. [[CrossRef](#)]
20. Song, Y.; Cai, L.; Tian, Z.; Wu, Y.; Chen, J. Phytochemical Curcumin-Coformulated, Silver-Decorated Melanin-like Polydopamine/Mesoporous Silica Composites with Improved Antibacterial and Chemotherapeutic Effects against Drug-Resistant Cancer Cells. *ACS Omega* **2020**, *5*, 15083–15094. [[CrossRef](#)]
21. Song, Y.; Zhu, P.; Xu, Z.; Chen, J. Dual-Responsive Dual-Drug-Loaded Bioinspired Polydopamine Nanospheres as an Efficient Therapeutic Nanoplatfrom against Drug-Resistant Cancer Cells. *ACS Appl. Bio Mater.* **2020**, *3*, 5730–5740. [[CrossRef](#)] [[PubMed](#)]
22. Bale, S.; Khurana, A.; Reddy, A.S.S.; Singh, M.; Godugu, C. Overview on Therapeutic Applications of Microparticulate Drug Delivery Systems. *Crit. Rev. Ther. Drug Carr. Syst.* **2016**, *33*, 309–361. [[CrossRef](#)] [[PubMed](#)]
23. Freiberg, S.; Zhu, X. Polymer microspheres for controlled drug release. *Int. J. Pharm.* **2004**, *282*, 1–18. [[CrossRef](#)] [[PubMed](#)]
24. Gaba, B.; Fazil, M.; Ali, A.; Baboota, S.; Sahni, J.K.; Ali, J. Nanostructured lipid (NLCs) carriers as a bioavailability enhancement tool for oral administration. *Drug Deliv.* **2015**, *22*, 691–700. [[CrossRef](#)] [[PubMed](#)]
25. Li, L.; Gu, Z.; Gu, W.; Liu, J.; Xu, Z.P. Efficient drug delivery using SiO<sub>2</sub>-layered double hydroxide nanocomposites. *J. Colloid Interface Sci.* **2016**, *470*, 47–55. [[CrossRef](#)]
26. Ding, A.; Teng, L.; Zhou, Y.; Chen, P.; Nie, W. Synthesis and characterization of bovine serum albumin-loaded microspheres based on star-shaped PLLA with a xylitol core and their drug release behaviors. *Polym. Bull.* **2018**, *75*, 2917–2931. [[CrossRef](#)]
27. Hariyadi, D.M.; Islam, N. Current Status of Alginate in Drug Delivery. *Adv. Pharmacol. Pharm. Sci.* **2020**, *2020*, 8886095. [[CrossRef](#)]
28. Tao, F.; Ma, S.; Tao, H.; Jin, L.; Luo, Y.; Zheng, J.; Xiang, W.; Deng, H. Chitosan-based drug delivery systems: From synthesis strategy to osteomyelitis treatment—A review. *Carbohydr. Polym.* **2021**, *251*, 117063. [[CrossRef](#)]
29. Zhang, K.; Tang, X.; Zhang, J.; Lu, W.; Lin, X.; Zhang, Y.; Tian, B.; Yang, H.; He, H. PEG-PLGA copolymers: Their structure and structure-influenced drug delivery applications. *J. Control. Release* **2014**, *183*, 77–86. [[CrossRef](#)]
30. Lin, X.-F.; Kankala, R.K.; Tang, N.; Xu, P.-Y.; Hao, L.-Z.; Yang, D.-Y.; Wang, S.-B.; Zhang, Y.S.; Chen, A.-Z. Supercritical Fluid-Assisted Porous Microspheres for Efficient Delivery of Insulin and Inhalation Therapy of Diabetes. *Adv. Healthc. Mater.* **2019**, *8*, 23546–23557. [[CrossRef](#)]
31. Yang, F.; Niu, X.; Gu, X.; Xu, C.; Wang, W.; Fan, Y. Biodegradable Magnesium-Incorporated Poly(L-lactic acid) Microspheres for Manipulation of Drug Release and Alleviation of Inflammatory Response. *ACS Appl. Mater. Interfaces* **2019**, *11*, 23546–23557. [[CrossRef](#)] [[PubMed](#)]
32. Yao, J.; Zhang, S.; Li, W.; Du, Z.; Li, Y. In vitro drug controlled-release behavior of an electrospun modified poly(lactic acid)/bacitracin drug delivery system. *RSC Adv.* **2016**, *6*, 515–521. [[CrossRef](#)]
33. Margulis, K.; Magdassi, S.; Lee, H.S.; Macosko, C.W. Formation of curcumin nanoparticles by flash nanoprecipitation from emulsions. *J. Colloid Interface Sci.* **2014**, *434*, 65–70. [[CrossRef](#)] [[PubMed](#)]
34. Pinon-Segundo, E.; Nava-Arzaluz, M.G.; Lechuga-Ballesteros, D. Pharmaceutical polymeric nanoparticles prepared by the double emulsion- solvent evaporation technique. *Recent Pat. Drug Deliv. Formul.* **2012**, *6*, 224–235. [[CrossRef](#)]
35. Zheng, W. A water-in-oil-in-oil-in-water (W/O/O/W) method for producing drug-releasing, double-walled microspheres. *Int. J. Pharm.* **2009**, *374*, 90–95. [[CrossRef](#)]

36. Esfandiari, N. Production of micro and nano particles of pharmaceutical by supercritical carbon dioxide. *J. Supercrit. Fluids* **2015**, *100*, 129–141. [[CrossRef](#)]
37. Pathak, P.; Meziat, M.J.; Desai, T.; Sun, Y.-P. Formation and stabilization of ibuprofen nanoparticles in supercritical fluid processing. *J. Supercrit. Fluids* **2006**, *37*, 279–286. [[CrossRef](#)]
38. Cocero, M.J.; Martin, A.; Mattea, F.; Varona, S. Encapsulation and co-precipitation processes with supercritical fluids: Fundamentals and applications. *J. Supercrit. Fluids* **2009**, *47*, 546–555. [[CrossRef](#)]
39. Xiao, Y.; Wu, Z.; Meng, Z.; Wang, Y.; Li, Z.; Zhao, Z. Synthesis of curcumin and indocyanine green co-loaded PLLA microparticles via solution-enhanced dispersion using supercritical CO<sub>2</sub> for chemo-photothermal therapy of osteosarcoma. *J. Supercrit. Fluids* **2022**, *180*, 105462. [[CrossRef](#)]
40. Champeau, M.; Thomassin, J.M.; Tassaing, T.; Jerome, C. Drug loading of polymer implants by supercritical CO<sub>2</sub> assisted impregnation: A review. *J. Control. Release* **2015**, *209*, 248–259. [[CrossRef](#)]
41. Reverchon, E.; Adami, R.; Caputo, G.; De Marco, I. Spherical microparticles production by supercritical antisolvent precipitation: Interpretation of results. *J. Supercrit. Fluids* **2008**, *47*, 70–84. [[CrossRef](#)]
42. Liu, Y.; Bhattarai, P.; Dai, Z.; Chen, X. Photothermal therapy and photoacoustic imaging via nanotheranostics in fighting cancer. *Chem. Soc. Rev.* **2019**, *48*, 2053–2108. [[CrossRef](#)] [[PubMed](#)]
43. Ban, Q.; Bai, T.; Duan, X.; Kong, J. Noninvasive photothermal cancer therapy nanoplatfoms via integrating nanomaterials and functional polymers. *Biomater. Sci.* **2017**, *5*, 190–210. [[CrossRef](#)] [[PubMed](#)]
44. Chu, K.F.; Dupuy, D.E. Thermal ablation of tumours: Biological mechanisms and advances in therapy. *Nat. Rev. Cancer* **2014**, *14*, 199–208. [[CrossRef](#)]
45. Song, X.; Chen, Q.; Liu, Z. Recent advances in the development of organic photothermal nano-agents. *Nano Res.* **2015**, *8*, 340–354. [[CrossRef](#)]
46. Xi, Y.; Ge, J.; Wang, M.; Chen, M.; Niu, W.; Cheng, W.; Xue, Y.; Lin, C.; Lei, B. Bioactive Anti-inflammatory, Antibacterial, Antioxidative Silicon-Based Nanofibrous Dressing Enables Cutaneous Tumor Photothermo-Chemo Therapy and Infection-Induced Wound Healing. *ACS Nano* **2020**, *14*, 2904–2916. [[CrossRef](#)]
47. Poinard, B.; Neo, S.Z.Y.; Yeo, E.L.L.; Heng, H.P.S.; Neoh, K.G.; Kah, J.C.Y. Polydopamine Nanoparticles Enhance Drug Release for Combined Photodynamic and Photothermal Therapy. *ACS Appl. Mater. Interfaces* **2018**, *10*, 21125–21136. [[CrossRef](#)]
48. Peng, Y.; Nie, J.; Cheng, W.; Liu, G.; Zhu, D.; Zhang, L.; Liang, C.; Mei, L.; Huang, L.; Zeng, X. A multifunctional nanoplatfom for cancer chemo-photothermal synergistic therapy and overcoming multidrug resistance. *Biomater. Sci.* **2018**, *6*, 1084–1098. [[CrossRef](#)]
49. Chen, Y.; Yu, Z.; Zheng, K.; Ren, Y.; Wang, M.; Wu, Q.; Zhou, F.; Liu, C.; Liu, L.; Song, J.; et al. Degradable mesoporous semimetal antimony nanospheres for near-infrared II multimodal theranostics. *Nat. Commun.* **2022**, *13*, 539. [[CrossRef](#)]
50. Zheng, Q.; Lin, T.; Wu, H.; Guo, L.; Ye, P.; Hao, Y.; Guo, Q.; Jiang, J.; Fu, F.; Chen, G. Mussel-inspired polydopamine coated mesoporous silica nanoparticles as pH-sensitive nanocarriers for controlled release. *Int. J. Pharm.* **2014**, *463*, 22–26. [[CrossRef](#)]
51. Pierini, F.; Nakielski, P.; Urbanek, O.; Pawlowska, S.; Lanzi, M.; De Sio, L.; Kowalewski, T.A. Polymer-Based Nanomaterials for Photothermal Therapy: From Light-Responsive to Multifunctional Nanoplatfoms for Synergistically Combined Technologies. *Biomacromolecules* **2018**, *19*, 4147–4167. [[CrossRef](#)] [[PubMed](#)]
52. Chen, P.; Wang, H.; Yang, F.; Chen, H.; He, W.; Wang, J. Curcumin Promotes Osteosarcoma Cell Death by Activating miR-125a/ERR Signal Pathway. *J. Cell. Biochem.* **2017**, *118*, 74–81. [[CrossRef](#)] [[PubMed](#)]
53. Wang, Z.; Zhang, K.; Zhu, Y.; Wang, D.; Shao, Y.; Zhang, J. Curcumin inhibits hypoxia-induced proliferation and invasion of MG-63 osteosarcoma cells via downregulating Notch1. *Mol. Med. Rep.* **2017**, *15*, 1747–1752. [[CrossRef](#)] [[PubMed](#)]
54. Jaque, D.; Maestro, L.M.; Rosal, B.D.; Haro-Gonzalez, P.; Benayas, A.; Plaza, J.L.; Rodríguez, E.; Nanoscale, J.S.J. Nanoparticles for photothermal therapies. *Nanoscale* **2014**, *6*, 9494–9530. [[CrossRef](#)]